Numerical calculation of path integrals: The small-polaron model

Hans De Raedt
Physics Department, University of Antwerp (Universitaire Instelling Antwerpen), Universiteitsplein 1, B-2610 Wilrijk, Belgium

Ad Lagendijk
Natuurkundig Laboratorium, Universteit van Amsterdam, Valckenierstraat 65, 1018-XE Amsterdam, The Netherlands
(Received 19 November 1982)

The thermodynamic properties of the small-polaron model are studied by means of a discrete version of the Feynman path-integral representation of the partition function. This lattice model describes a fermion interacting with a boson field. The bosons are treated analytically, the fermion contribution is calculated using a Monte Carlo method. We analyze the thermodynamic functions for the case of one-, two-, and three-dimensional polaron motion. We present strong evidence that the polaron becomes superlocalized if the interaction strength is greater than a critical value.

I. INTRODUCTION

Phase transitions and phase diagrams of the ground state of quantum systems are essential for the characterization of the general behavior of these models. A special class of interesting problems is the coupled fermion-boson system. In this paper we want to discuss a lattice model in which one fermion is coupled to a boson field, a polaron. In solids and liquids the polaron is a fundamental concept. The polaron is an electron which is coupled to lattice vibrations, the bare electron is dressed by phonons. Here we report the results of an extensive Monte Carlo study of the thermodynamics of a small polaron.[1] This polaron is described by the Holstein Hamiltonian [see (2.1)], a lattice model originating from a tight-binding Hamiltonian.[2–4] There have been many speculations about a possible phase transition connected with localization of the electron as a function of the electron-phonon coupling constant in continuum polaron models.[5] However, for the most interesting continuum model, the Fröhlich polaron, Feynman, using his path-integral formalism, has given a superior solution for the ground-state energy which does not exhibit any discontinuities.[6] The value for the coupling constant where the Fröhlich polaron is supposed to change the character of its ground state occurs at values where the continuum picuture is expected to break down for real systems. Localization is also possible for the small polaron. For small values of the coupling constant the motion of this polaron is bandlike, whereas for large values of the coupling constant the polaron exhibits hoppinglike motion. As a matter of fact, usually only the latter regime is referred to as the small polaron, but we will use the notion of small polaron in the more general context. In most cases the term localization is restricted to phenomena occurring in random systems where it concerns the character of the wave function as a function of some randomness parameter. In random systems there is no symmetry and localization is not connected with symmetry breaking. In uniform lattice models such as the polaron model the translational symmetry can be broken, in principle. There is no evidence that this will happen for this one-body problem, and we are concerned with localization effects which conserve translational symmetry. These effects are described by correlation functions which measure the spatial extent of the lattice distortion caused by the electron.

Our method uses the generalized Trotter formula to generate a discrete version of the Feynman path integral. With the use of this particular path integral the dispersionless phonons can be integrated out and we are left with a $(d+1)$-dimensional classical system. This system is simulated with the help of the standard Monte Carlo technique.[7–9]

Our results point to substantially enhanced fluctuations in the neighborhood of a critical value of the coupling constant for all lattice dimensionalities (1, 2, and 3). The fluctuations are found in correlations which are sensitive to the localized character of the polaron. We have monitored operators which could serve as order parameters since the expectation value of these observables is drastically reduced once the strong-coupling regime is entered.

The paper is organized as follows. In Sec. II we

present the underlying theory and we derive expressions for the observable quantities in terms of path integrals. In Sec. III we discuss the computational technique used to calculate the path integral and we also compare our approach with others. A discussion of the simulation data for the polaron is given in Sec. IV. The conclusions drawn from these calculations can be found in Sec. V.

II. THEORY

We assume that the fermion moves in a d-dimensional hypercube of linear size N and that there is only one boson degree of freedom per site. We will take an Einstein model for the lattice vibrations. In principle, the theory given below can be extended to the case of phonons with dispersion. In the analytic manipulations only a few slight modifications in the notations would be required, but owing to dependence on the spatial dimensionality, additional numerical calculations of integrals over the Brillouin zone would be necessary. We prefer to study the more simple dispersionless polaron model because the emphasis of this work is on the calculational method of the thermodynamic properties. For simplicity of notation we will now formulate the theory in one space dimension. The formulas for two-dimensional (2D) and three-dimensional (3D) systems can be derived by means of the same technique but we will not present them here. The model Hamiltonian reads

$$H = H_0 + H_1 + H_2 , \tag{2.1a}$$

$$H_0 = \frac{1}{2M} \sum_{i=1}^{N} p_i^2 , \tag{2.1b}$$

$$H_1 = \frac{M\Omega^2}{2} \sum_{i=1}^{N} x_i^2 + \lambda \sum_{i=1}^{N} x_i c_i^\dagger c_i , \tag{2.1c}$$

$$H_2 = -t \sum_{i=1}^{N} c_i^\dagger c_{i+1} + c_{i+1}^\dagger c_i . \tag{2.1d}$$

The mass M will usually been taken to be 1, Ω is the angular frequency of the Einstein oscillator, λ is the fermion-boson coupling strength, and t is the kinetic energy associated with the nearest-neighbor hopping motion of the fermion. The momentum and coordinate of the ith boson are denoted by p_i and x_i, $c_i^\dagger$ creates a fermion at site i, c_i removes a fermion from site i.

The Hamiltonian (2.1) describes an electron coupled linearly to the phonon field of the site where the electron resides. The phonons are dispersionless and consequently the only intersite communication is through the electron. Physical realizations of the d-dimensional model could be found in molecular crystals. One needs a molecular unit compatible with the lattice symmetry and having a nondegenerate internal mode, for instance, the breathing mode.

To derive a path-integral representation of the partition function we use the Trotter formula[10] and obtain

$$Z \equiv \mathrm{Tr} e^{-\beta H} = \lim_{m \to \infty} Z_m , \tag{2.2a}$$

$$Z_m = \mathrm{Tr}(e^{-\tau H_0} e^{-\tau H_1} e^{-\tau H_2})^m , \tag{2.2b}$$

where $\tau = \beta/m$. The Hamiltonians H_0 and H_2 describe free particles and can be diagonalized by inspection. Furthermore, H_1 is diagonal in the coordinate representation of the boson field and fermion position. Substituting the spectral representation of these operators in (2.2) and working out all resulting matrix elements, we can evaluate the integrals over all boson and fermion momenta analytically. We obtain

$$Z_m = c_1 \tau^{-mN/2} \sum_{\{y_j\}} \int \left[\prod_{j=1}^{m} \prod_{n=1}^{N} dx_{nj} \right] \left[e^{-S^B} \prod_{j=1}^{m} I(2\tau t, y_j - y_{j+1}) \right] , \tag{2.3a}$$

where

$$S^B = \sum_{j=1}^{m} \sum_{n=1}^{N} \left[\frac{1}{2\tau}(x_{nj} - x_{nj+1})^2 + \frac{\tau\Omega^2}{2} x_{nj}^2 + \tau\lambda x_{nj} \delta_{n,y_j} \right] . \tag{2.3b}$$

Here c_1 is an unimportant constant factor and y_j denotes the position of the fermion on the jth replica of the original chain. The index j labels the number of complete sets of states that have been inserted in (2.2b) and plays the same role as the imaginary-time variable appearing in the path integral.[6,11] The model has been formulated on a lattice and hence the fermion kinetic energy is not represented by a Gaussian but by a Fourier-transformed imaginary-time lattice propagator

$$I(z,l) = \frac{1}{N} \sum_{n=1}^{N} \cos\frac{2\pi l n}{N} \times \exp\left[-z \cos\frac{2\pi n}{N} \right] . \tag{2.4}$$

In the limit $N\to\infty$ this function is nothing but the modified Bessel function of the first kind of order l. For consistency we use the discrete lattice sum instead of the Bessel function.

Because S^B is quadratic in the boson coordinates we can carry out the integration over all x_{nj}. Here we will first diagonalize the quadratic boson action by means of a discrete Fourier transformation with respect to the variable j. Alternatively one could start from the continuum limit of the boson action, but this is inconsistent with the discretization procedure used for the fermion. We have chosen a simple Einstein model for the bosons and therefore it is possible to integrate out each boson degree of freedom separately. We set

$$x_{nj}=\frac{1}{\sqrt{m}}\sum_{k=0}^{m-1} v_{nk}\exp\left[\frac{2\pi jk}{m}\right] \tag{2.5a}$$

and obtain

$$S^B=\sum_{n=1}^{N}\sum_{k=0}^{m-1}\left[\frac{1}{\tau}a_k^{-1}|v_{nk}|^2+\frac{\tau\lambda v_{nk}}{\sqrt{m}}\sum_{j=1}^{m}\delta_{n,y_j}\exp\left[\frac{2\pi jk}{m}\right]\right], \tag{2.5b}$$

where

$$a_k=1-\cos\frac{2\pi k}{m}+\frac{\tau^2\Omega^2}{2} \tag{2.5c}$$

is the inverse of the free-boson propagator. Integrating out all the v_{nk} yields

$$Z_m=c_2Z_m^BZ_m^F\,, \tag{2.6a}$$

$$Z_m^B=\left[\prod_{k=0}^{m-1}a_k^{-1/2}\right]^N, \tag{2.6b}$$

$$Z_m^F=\sum_{\{y_j\}}\rho(y_j)\,, \tag{2.6c}$$

$$\rho(y_j)=\left[\prod_{j=1}^{m}I(2\tau t,y_j-y_{j+1})\right]\times\exp\left[\sum_{i=1}^{m}\sum_{j=1}^{m}F(i-j)\delta_{y_i,y_j}\right], \tag{2.6d}$$

$$F(l)=\frac{\tau^3\lambda^2}{4m}\sum_{k=0}^{m-1}a_k^{-1}\cos\frac{2\pi kl}{m}\,. \tag{2.6e}$$

All unimportant numerical factors have been absorbed in c_2. The approximant Z_m^B to the partition function of the free-boson system can be calculated exactly. A detailed discussion is given in Appendix A. The calculation of the fermion contribution Z_m^F is a nontrivial problem because the density function $\rho(y_j)$ describes a peculiar 2D classical system of m particles at the positions y_j interacting with each other. The first factor in (2.6d) represents an effective nearest-neighbor interaction, the second accounts for the retarded long-range interactions caused by the fermion-boson coupling. In each row the real-space direction contains one electron interacting with the electrons in other rows.

Obviously, (2.6c) will reproduce the exact free-fermion results for any value of m if the fermion-boson coupling $\lambda=0$. In general, it can be shown that $Z_m\geq Z_{m+1}\geq Z$.[12] Therefore, the approach used here will give us lower bounds on the free energy instead of the upper bounds obtained by conventional variational methods.

The function Z_m^F itself is not useful; more relevant are the approximants to the energy, specific heat, and derivatives of the free energy $F_m^F=-(1/\beta)\ln Z_m^F$ with respect to the coupling λ. To simplify the notation a little bit, we will denote the expectation value of a quantity A taken in the ensemble defined by the density function $\rho(y_j)$ by

$$\langle A\rangle\equiv\frac{1}{Z_m^F}\sum_{\{y_j\}}\rho(y_j)A(y_j)\,. \tag{2.7}$$

We have

$$E_m^F\equiv-\frac{\partial}{\partial\beta}\ln Z_m^F=K_m^F+V_m^F\,, \tag{2.8a}$$

$$K_m^F=-\frac{1}{m}\sum_{j=1}^{m}\left\langle\frac{I(2\tau t,y_j-y_{j+1}-1)+I(2\tau t,y_j-y_{j+1}+1)}{I(2\tau t,y_j-y_{j+1})}\right\rangle, \tag{2.8b}$$

$$V_m^F=-\frac{1}{m}\sum_{i=1}^{m}\sum_{j=1}^{m}\frac{\partial F(i-j)}{\partial\tau}\langle\delta_{y_i,y_j}\rangle\,, \tag{2.8c}$$

where K_m^F and V_m^F stand for kinetic and interaction energy. The fermion contribution to the specific heat is given by

$$C_m^F\equiv-\beta^2\frac{\partial}{\partial\beta}E_m^F=2\tau t\beta-(\beta E_m^F)^2+\tau^2[\langle(e_m^F)^2\rangle+\langle c_m^F\rangle]\,, \tag{2.9a}$$

$$e_m^F=\sum_{j=1}^{m}\frac{I(2\pi t,y_j-y_{j+1}-1)+I(2\pi t,y_j-y_{j+1}+1)}{I(2\pi t,y_j-y_{j+1})}+\sum_{i=1}^{m}\sum_{j=1}^{m}\frac{\partial F(i-j)}{\partial\tau}\delta_{y_i,y_j}\,, \tag{2.9b}$$

$$c_m^F=\sum_{j=1}^{m}\frac{I(2\pi t,y_j-y_{j+1}-2)+I(2\pi t,y_j-y_{j+1}+2)}{I(2\pi t,y_j-y_{j+1})}$$
$$-\sum_{j=1}^{m}\left[\frac{I(2\pi t,y_j-y_{j+1}-1)+I(2\pi t,y_j-y_{j+1}+1)}{I(2\pi t,y_j-y_{j+1})}\right]^2+\sum_{i=1}^{m}\sum_{j=1}^{m}\frac{\partial^2F(i-j)}{\partial\tau^2}\delta_{y_i,y_j}\,. \tag{2.9c}$$

Here we used the recursion relation $2\partial I(z,l)/\partial z=I(z,l-1)+I(z,l+1)$. Straightforward algebra yields

$$\frac{\partial F_m^F}{\partial\lambda}=\hat{C}(0)\equiv-\frac{2}{\beta\lambda}\sum_{i=1}^{m}\sum_{j=1}^{m}F(i-j)\langle\delta_{y_i,y_j}\rangle\,, \tag{2.10a}$$

$$\lim_{m\to\infty}\frac{\partial F_m^F}{\partial\lambda}=\sum_{i=1}^{N}\frac{\mathrm{Tr}e^{-\beta H}c_i^\dagger c_i x_i}{\mathrm{Tr}e^{-\beta H}}\,, \tag{2.10b}$$

and

$$\frac{\partial^2F_m^F}{\partial\lambda^2}=-\frac{4}{\beta\lambda^2}\sum_{i=1}^{m}\sum_{j=1}^{m}\sum_{i'=1}^{m}\sum_{j'=1}^{m}F(i-j)F(i'-j')\times\langle\delta_{y_i,y_j}\delta_{y_{i'},y_{j'}}\rangle$$
$$-\frac{1}{\lambda}\frac{\partial F_m^F}{\partial\lambda}+\beta\left[\frac{\partial F_m^F}{\partial\lambda}\right]^2. \tag{2.10c}$$

The first derivative of the free energy (2.10a) is related to the expectation value of the operator $\sum_i x_i c_i^\dagger c_i$, the second derivative (2.10c) is proportional to the static susceptibility of this quantity. It will turn out that it is more interesting to study the fluctuations of $\partial F_m^F/\partial\lambda$ and, therefore, it is useful to introduce the function

$$\Delta F_m^F=\frac{\partial^2F_m^F}{\partial\lambda^2}+\frac{1}{\lambda}\frac{\partial F_m^F}{\partial\lambda}\,. \tag{2.11}$$

A discontinuity in $\partial F_m^F/\partial\lambda$ or ΔF_m^F as a function of λ means that the free energy is not an analytic function of the coupling λ and, in analogy with the theory of phase transitions, this indicates that the system undergoes a transition.

In order to gain additional insight in the properties of the model it is useful to consider fermion-boson correlation functions. After some algebraic manipulations we find

$$\lim_{m\to\infty}\hat{C}(l)=\sum_{i=1}^{N}\frac{\mathrm{Tr}e^{-\beta H}c_i^\dagger c_i x_{i+1}}{\mathrm{Tr}e^{-\beta H}}\,, \tag{2.12a}$$

where

$$\hat{C}(l)\equiv-\frac{2}{\beta\lambda}\sum_{i>j=1}^{m}F(i-j)\langle\delta_{|y_i-y_j|,l}\rangle\,, \tag{2.12b}$$

if $l\neq0$. For $l=0$ we should use expression (2.10a). It is convenient to introduce the normalized fermion-boson correlation function

$$C(l)\equiv\hat{C}(l)/\hat{C}(0)\,. \tag{2.12c}$$

Studying $C(l)$ as a function of the coupling λ will give us direct information about the way the fermion distorts its surrounding.

III. CALCULATIONS

The formalism presented in the preceding section is of little use unless we can calculate the quantities (2.8)—(2.12) for different values of m, β, t, and λ (for convenience we have chosen units such that $\Omega=1$). Although in a strict sense the density function (2.7) is not a density function of a genuine 2D classical model, we can still use the standard classical Monte Carlo method[7–9] to estimate the expectation values within a certain statistical accuracy. By doing so we avoid approximations such as perturbation expansions or variational procedures. Of course, perturbation expansions and variational methods are very useful to calibrate the simulation data. Therefore, we calculated the first nontrivial weak coupling correction to the fermion energy (see Appendix B) and we will also compare our data with the strong coupling results.

It should be clear that one fundamental approximation has already been made by keeping m finite. Therefore, it is necessary to study the convergence of the results as a function of m. For the boson contribution Z_m^B the convergence can be studied rigorously as is shown in Appendix A. From this study we can deduce a minimum value of m such that for each inverse temperature β the exact results of the boson system are reproduced within a specified error. The actual value of m used in the simulations depends on the value of β, t, and λ and is determined such that within the statistical errors of the simulations, the results remain the same if m increases any further.

We now summarize some technical details of the

simulation. To check our program we reproduced the exact results for 1D, 2D, and 3D noninteracting systems of different sizes and several values of β, t, and m. In our opinion this should always be done first. It gives some indication that the phase space is sampled correctly. Any Monte Carlo method that fails to pass this simple but essential test can not be trusted. In our final simulations, we chose $N=32$ (a variation of the linear dimension N only has a very small effect on the results) and $2000m$ single-particle steps were discarded before taking samples. Most of the data presented here have been obtained from runs of 50 000 samples each. The number of single-particle steps between two successive samples is m. Occasionally longer runs have been made to convince ourselves that there were no systematic errors. The choice of the initial configuration has a negligible effect on the results. It turns out that the specific heat is the most difficult quantity to sample, especially at low temperature. The statistical errors on the specific heat are somewhat larger than those on the other quantities but there is the additional problem that it is also more sensitive to the choice of m. The same problem also occurs in other models. For the harmonic oscillator the exact analysis of Appendix A demonstrates that the convergence of C_m^B as a function of m is much slower than that of E_m^B (see Table I). The same behavior has been observed in exact short-chain calculations for 1D fermion systems.[13] Therefore, it might well be that it is a general property of the Trotter formula which makes the calculation of the specific heat at low temperatures more difficult. The main source of statistical fluctuations comes from quantities related to the kinetic energy H_2. This could be expected because we are simulating a quantum model in real space instead of in momentum space. A typical run ($d=1$, $\beta=5$, $N=32$, $m=32$, $t=1$, and $\lambda=3$) takes 40 minutes of CPU (central processing unit) time on a Digital Equipment Corporation VAX11/780 computer.

We close this section by comparing our method[13] with other attempts to use Monte Carlo simulations to study fermion-boson models.[14] The analytic elimination of the boson degrees of freedom simplifies considerably the problem of calculating the thermodynamic properties. In the first place, we have formulated the fermion-boson problem in such a way that the fermion contribution can be calculated separately. Therefore, we are able to study the fermion properties quantitatively. This is in sharp contrast to another formulation[14] in which not only the fermion but also the boson properties are calculated simultaneously by some simulation technique. In such an approach the polaron contribution is hidden in the statistical noise of the bosons because in the approximation to the functional integral there are mN^d boson variables while there are only md fermion degrees of freedom. Furthermore, in that method the number of variables grows exponentially

TABLE I. Comparison between two approximations to the path integral of a harmonic oscillator. Exact results correspond to $m=\infty$. Energy E_m^B and specific heat C_m^B have been calculated using the simplest discretization procedure of the path integral. Continuum form of the path integral and a trigonometric approximation have been used to calculate the energy e_m and specific heat c_m. Oscillator frequency $\Omega=1$ and the temperature is very low ($\beta=5$).

m	E_m^B	C_m^B	e_m	c_m
2	0.321 95	1.133 79	0.264 85	0.886 03
3	0.392 31	0.963 02	0.342 39	0.798 96
4	0.431 62	0.769 18	0.374 69	0.742 25
5	0.454 55	0.619 83	0.402 03	0.642 93
6	0.468 71	0.513 42	0.418 38	0.585 08
7	0.477 94	0.438 03	0.431 53	0.527 99
8	0.484 24	0.383 77	0.440 78	0.489 04
9	0.488 72	0.343 87	0.448 39	0.453 86
10	0.492 00	0.313 87	0.454 24	0.427 49
12	0.496 37	0.272 87	0.463 18	0.385 32
14	0.499 07	0.247 03	0.469 54	0.354 82
16	0.500 85	0.229 79	0.474 29	0.331 79
18	0.502 07	0.217 75	0.477 96	0.313 83
20	0.502 96	0.209 02	0.480 90	0.299 44
24	0.504 12	0.197 51	0.485 28	0.277 84
28	0.504 82	0.190 49	0.488 40	0.262 42
32	0.505 28	0.185 91	0.490 72	0.250 87
∞	0.506 78	0.170 74	0.506 78	0.170 74

with the spatial dimension d. Consequently it cannot be used to simulate the system of the linear size $N=32$ (which was the value of N used in most of our simulations) unless $d=1$ or the temperature is high (if $\beta=5$, m should be larger than 20 in order to have accurate results). An important advantage of our approach is that it combines analytic and numerical techniques in such a way that the simulation itself is very efficient. If we had not used the fact that the Hamiltonian is quadratic in x_{nj}, the number of variables in the partition function (2.6a) would be $m(N^d+1)$. Now, however, we can evaluate Z_m^B exactly and the number of variables in the sum Z_m^F is only m. In practice this implies that the computer time for the simulation only grows quadratic with m and linear with d. This allows us to make a systematic study of the convergence of the approximants as a function of m, rather than using intuition for choosing a particular value for m.[14] To summarize, it is now obvious that in our approach no additional numerical procedure is necessary to extract the relevant polaron properties from noisy data, it is very efficient from the point of view of computer time, and it is possible to study the model in all spatial dimensions.

IV. RESULTS

In Fig. 1 we plot the energy E_m^F and ΔF_m^F as a function of $1/m$ for $\beta=5$, $\lambda=3$, and $t=1$. It is clear that although the temperature is very low (see also the discussion in Appendix A), the convergence is rather good and a linear extrapolation scheme would give us an accurate estimate of the exact results $m\to\infty$. Keeping m and β constant and varying λ we obtain the data depicted in Fig. 2. For comparison we also show the weak coupling (B6) and strong coupling results for the energy. There is good agreement between the simulation data and the weak coupling theory as long as $\lambda<2$ and a similar conclusion holds for strong coupling $\lambda>3$. In the intermediate coupling regime $2<\lambda<3$ the curvature of $\partial F_m^F/\partial\lambda$ is very weak and $\partial^2 F_m^F/\partial\lambda^2$ has a maximum. Of course, it is impossible to rule out that there is a discontinuity in the first derivative by means of a numerical calculation, but in this case we do not have other evidence that might support this hypothesis. A more detailed picture of what is going on in this region is obtained by plotting the fluctuation ΔF_m^F. In Fig. 3 we compare the data of ΔF_m^F for different t and β. For $t=1$ (which was also the value of t in the previous figures) the maximum of ΔF_m^F is located at $\lambda\approx 2.6$. As the temperature in-

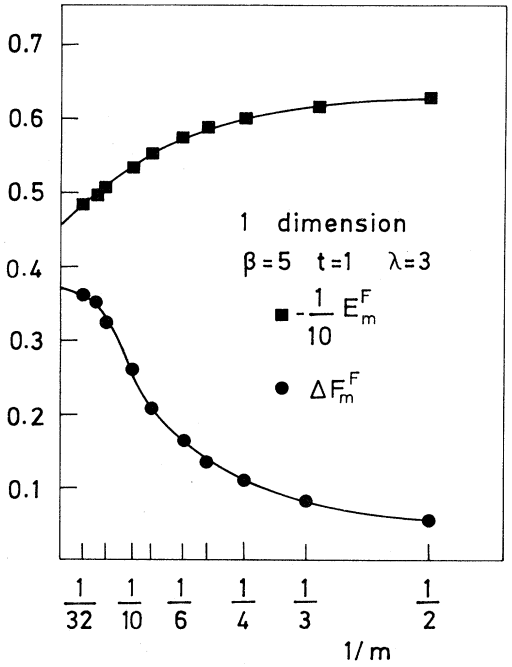

FIG. 1. Energy E_m^F and fluctuation ΔF_m^F at low temperature and constant coupling as a function of $1/m$. In all figures solid lines are guides to the eye only.

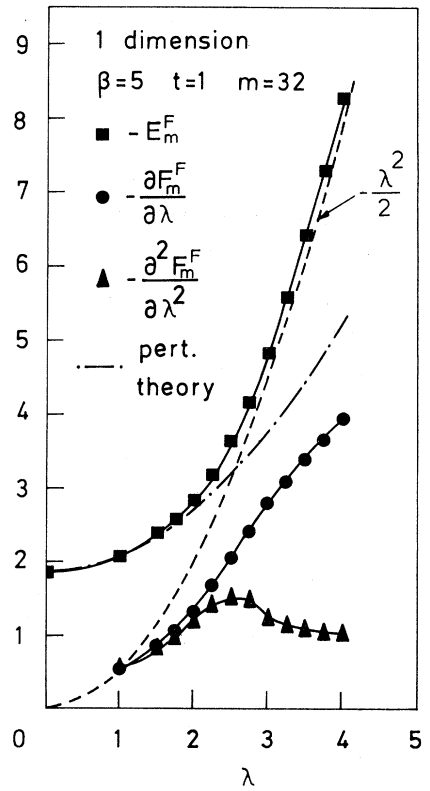

FIG. 2. Energy, the first derivative of the free energy with respect to λ, and the second derivative of the free energy with respect to λ as a function of the coupling λ. Also shown are the results of weak and strong coupling theories.

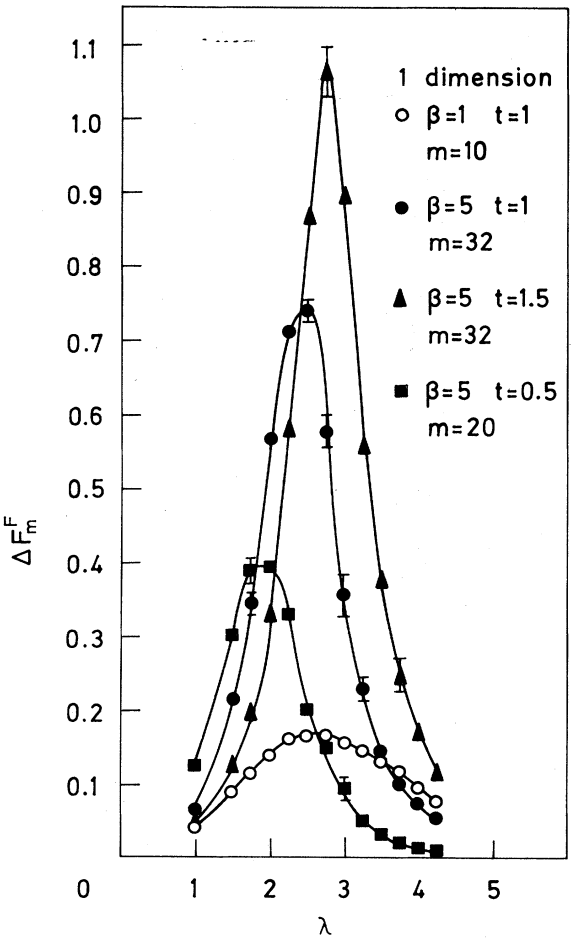

FIG. 3. Coupling dependence of the fluctuation ΔF_m^F for several temperatures and hopping energies t.

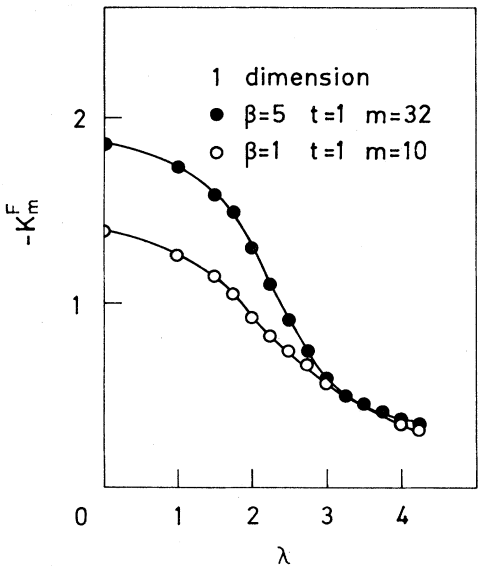

FIG. 4. Kinetic energy as a function of the coupling λ.

creases this maximum decreases rapidly but the peak position remains the same. If we keep the temperature constant ($\beta=5$) and vary the hopping energy t we see that the peak position and the peak height increase with increasing t. We observe that to a good approximation, the peak position λ_c can be found by equating the weak and strong coupling expansions of the ground-state energy. Converting the sum in (B7) into an integral we find

$$\lambda_c^2=4t[1-(1+4t)^{-1/2}]^{-1}\,. \tag{4.1}$$

The plots of the fluctuations seem to be symmetrical in the vicinity of λ_c, but because λ^2 rather than λ sets the scale of the coupling energy this behavior is not related to a physical property of the model. In Fig. 4 we show the kinetic energy as a function of λ at low and intermediate temperature. In the critical region where $\lambda\approx\lambda_c$ the absolute value of the kinetic energy decreases rapidly with increasing λ. The statistical errors increase if λ approaches its critical values, an effect which is also observed in Monte Carlo simulations of phase transitions.[9] To illustrate the high degree of accuracy that can be obtained by the technique used here, we also show (see Fig. 5) a comparison between the weak and (zero-temperature) strong coupling results and the simulation data of the energy E_m^F at intermediate temperature ($\beta=1$). The higher the temperature, the less is the value m (and computation time) that is needed to obtain the correct answers. This is an intrinsic property of the approximation (2.2b) as is also illustrated by comparing the data of Tables I and II. We see that, except for Fig. 1, the value of m used in the simulations is large enough to guarantee that the approximation (2.6b) for the bosons is very accurate.

A typical plot of the m dependence of E_m^F and ΔF_m^F in the case of 2D fermion motion is shown in Fig. 6. As in the 1D case, the rate of convergence of the approximants is quite good. In Fig. 7 we compare simulation data obtained at low temperature ($\beta=5$) for the energy of the 2D and 3D models with two types of ground-state energy calculations: second-order perturbation theory and a strong coupling approach. Results on ΔF_m^F for 2D and 3D fermion motion are given in Fig. 8. At low temperature $\beta=5$ we find a very sharp large peak in ΔF_m^F (note that there is a difference in scale between 2D and 3D data). The fluctuations ΔF_m^F are much larger than in the 1D case. In contrast to the 1D case, the most important contribution to $\partial^2 F_m^F/\partial\lambda^2$ [see (2.10c)] in the critical region is not $\partial F_m^F/\partial\lambda$ but ΔF_m^F. The fluctuation on the first derivative of the

TABLE II. Same as for Table I but here $\beta=1$.

m	E_m^B	C_m^B	e_m	c_m
2	1.0588	0.9481	1.0188	0.9818
3	1.0714	0.9336	1.0435	0.9583
4	1.0760	0.9281	1.0535	0.9489
5	1.0781	0.9255	1.0598	0.9427
6	1.0793	0.9240	1.0637	0.9389
7	1.0800	0.9231	1.0665	0.9361
8	1.0805	0.9225	1.0685	0.9341
9	1.0808	0.9221	1.0701	0.9325
10	1.0810	0.9219	1.0713	0.9313
12	1.0813	0.9215	1.0732	0.9294
14	1.0815	0.9213	1.0745	0.9281
16	1.0816	0.9211	1.0754	0.9272
18	1.0817	0.9210	1.0762	0.9264
20	1.0817	0.9209	1.0768	0.9258
24	1.0818	0.9208	1.0777	0.9249
28	1.0819	0.9208	1.0783	0.9243
32	1.0819	0.9207	1.0788	0.9238
∞	1.0820	0.9206	1.0820	0.9206

free energy with respect to the coupling λ has a very pronounced maximum at a certain value of the interaction parameter λ and this indicates that the system switches from one state to another if the coupling λ passes its critical value. As in the 1D model, these effects disappear as the temperature increases. In Fig. 9 we show the data for $-d^{-1}K_m^F$

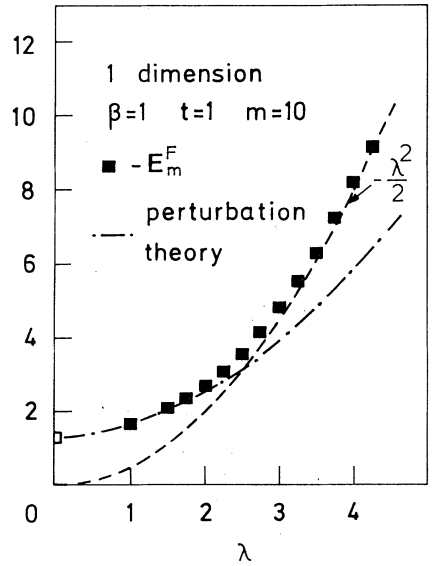

FIG. 5. Comparison between the weak and strong coupling theories and the simulation data for E_m^F at intermediate temperature $\beta=1$.

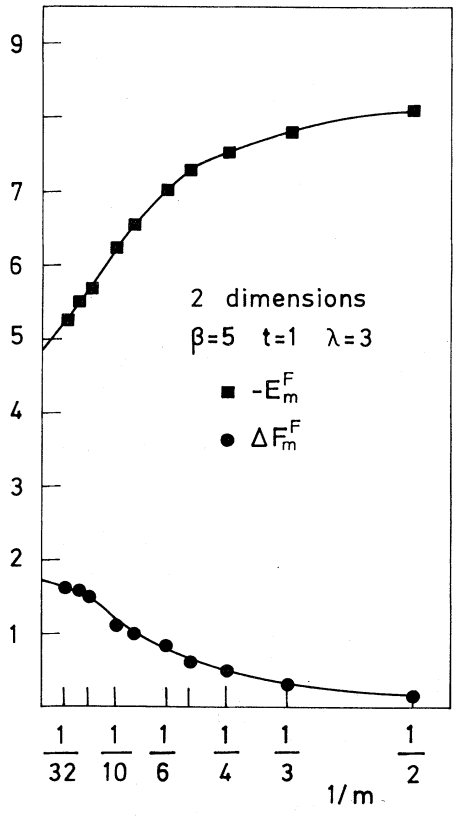

FIG. 6. Energy E_m^F and fluctuation ΔF_m^F at low temperature and constant coupling as a function of $1/m$. Fermion moves on a two-dimensional square lattice.

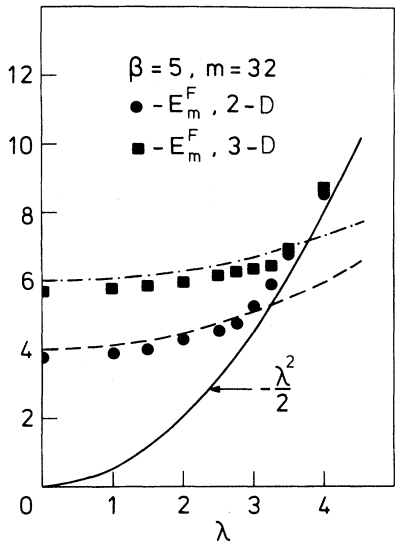

FIG. 7. Comparison between the *ground-state* energy (dashed line, 2D model; dash-dot line, 3D model) obtained from second-order perturbation theory, the energy in the strong coupling regime (solid line) and simulation data for E_m^F (solid dots, 2D model; solid squares, 3D model). Plot shows that in our units ($t=1$ and $\Omega=1$) the inverse temperature $\beta=5$ corresponds to a very low temperature for these systems.

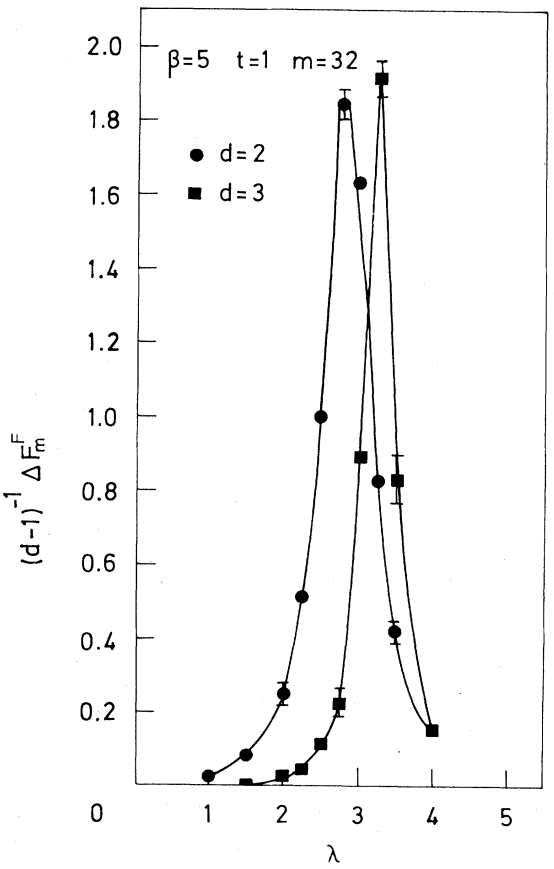

FIG. 8. Coupling dependence of the fluctuation ΔF_m^F at low temperature. Fermion moves on a 2D square lattice (dots) and on a 3D cubic lattice (squares). Note that the 3D results for ΔF_m^F are shown on a different scale.

and as in the 1D model we observe a rapid decrease of the kinetic energy as the coupling λ increases. In the critical region the kinetic energy of the 2D and 3D models drops more rapidly than in the 1D case. This is consistent with the observation that the transition in two and three dimensions is more abrupt than in one dimension.

In Fig. 10 we compare the normalized nearest-neighbor fermion-boson correlation functions (2.12) for 1D, 2D, and 3D polaron motion. We see that in all cases $C(\Delta)$ (Δ stands for a unit vector of the d-dimensional hypercube) decreases rapidly if the coupling λ increases toward its critical value. We have also calculated the more-distant correlation functions. We find that they display a similar behavior but the actual values decrease fast with distance. This, of course, is just the same as saying that the polaron is small.[2-4]

V. DISCUSSION

The general picture is quite clear. As the coupling grows, the polaron loses kinetic energy and it gains potential energy. This is a general charasteristic behavior for particles which become more and more localized. It is also clear from the results that there is a critical line in the (t,λ) plane. The critical points are recognized through a large growth of fluctuations. The observable connected with the coupling energy shows enhanced fluctuations and, in addition, there is the sharp drop in the order-parameter-type observable.

Several limits of the polaron model can be attacked with analytic tools. These limits are the weak coupling regime ($\lambda \ll t,\Omega$), the adiabatic regime ($M\to\infty$, $M\Omega^2$ finite), and the small-bandwidth limit ($t\to 0$).[2-4] The weak coupling calculation is straightforward (see Appendix B). One must be very careful with the adiabatic limit because it introduces a possible spurious breaking of the translational symmetry. A finite-body problem does not allow any symmetry breaking to occur. This can easily be seen by assuming the opposite. If we had prepared the system in a broken-symmetry state, other equivalent states could be generated by applying all the symmetry operations of the Hamiltonian. The probability for a transition from these

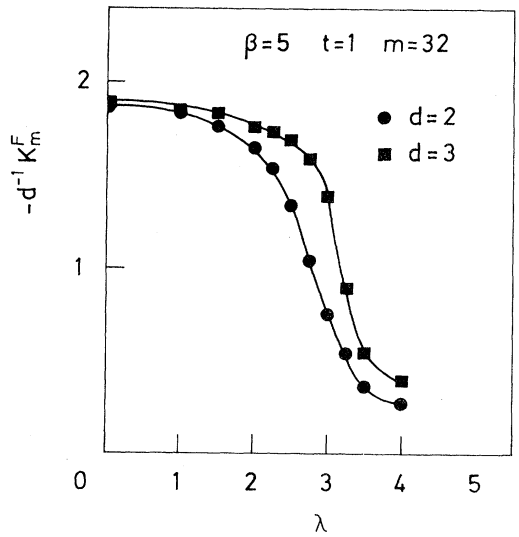

FIG. 9. Kinetic energy as a function of the coupling λ in the case of 2D and 3D fermion motion.

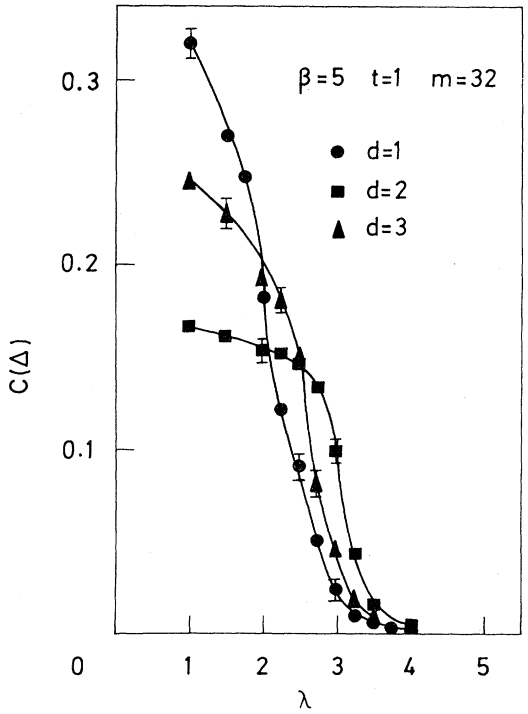

FIG. 10. Normalized nearest-neighbor fermion-boson correlation functions for 1D, 2D, and 3D polaron motion as a function of the coupling λ.

states to the broken-symmetry state is nonzero. Therefore, the latter can not be the ground state since the particle can tunnel to other states. A very large tunnel barrier would imply a very long lifetime, but this is not a critical effect. In an infinite-body theory the broken-symmetry state can be stable because its lifetime depends on macroscopic tunneling. However, a finite-body system can have order parameters which are not connected with any loss of symmetry.

The adiabatic limit has much in common with the one-impurity level in a tight-binding Hamiltonian treated in detail by Economou.[15] When $\lambda^2 > 4tM\Omega^2$ a bound state can be pulled out of the 1D continuum. The nonadiabatic corrections will restore the translational symmetry because the localized wave functions will become the local building blocks of Bloch-type wave functions. However, it is still very likely that the character of the wave function changes in the neighborhood of $\lambda^2 \approx 4tM\Omega^2$. This becomes even more apparent in the small-t limit. Holstein has obtained the highly nonadiabatic solutions in that case. The wave functions are superlocalized in the sense that any operator measuring the correlation between the electron and a phonon vanishes unless the correlation is measured on the same site. Nevertheless, the wave functions transform according to irreducible representations of the translation group. Holstein's result for the 1D case is

$$E(k) = -\frac{\lambda^2}{2M\Omega^2} - 2t\cos k \exp\left[-\frac{\lambda^2}{2M\Omega^3}\right]. \quad (5.1)$$

showing the reduction of the bandwidth with the exponential Huang-Rhys factor.[3] Of course, if the translational symmetry would be broken we would end up with a perfectly localized adiabatic solution. The hopping motion does not contribute to the energy in a significant way in the strong coupling regime, and that is why our strong coupling results in Figs. 2 and 5 are essentially the contribution $\lambda^2/2M\Omega^2$. In the weak coupling limit and in the adiabatic limit the size of the polaron extends over many sites with an exponential decay of correlation between the electron and the phonons. In the strong coupling regime the polaron is superlocalized and the extension of the polaron is over one site only. It is this transition that we are observing in our Monte Carlo experiments.

So far we have only discussed the ground-state properties. At finite temperatures all states become thermally available and all the effects discussed so far will flatten out. This is precisely what we observe in our simulations. In the strong coupling regime there is supposed to be an interesting change of transport properties as a function of temperature.[2] At a suitable temperature the electron can hop over the barrier due to its thermal energy. Unfortunately, these dynamic phenomena are not directly measurable by the techniques used in the present

work. These dynamic effects have no drastic influence on the thermodynamic properties discussed in this paper.

In the preceding discussion we have implicitly assumed that we were dealing with the 1D case. In two and three dimensions we find the same features as for the 1D polaron. In the strong coupling limit the small polaron behaves, effectively, as a zero-dimensional system, and the behavior of the system is insensitive to the lattice dimensionality. The general tendency seems to be that the critical region becomes smaller and the transition is more abrupt.

ACKNOWLEDGMENTS

We would like to thank J. Fivez for many fruitful discussions and a critical reading of the manuscript. This work is supported by the Belgian Interuniversitair Instituut voor Kernwetenschappen and the Dutch Stichting voor Fundamenteel Onderzoek der Materie.

APPENDIX A

In this section we examine the approximant Z_m^B to the partition function of a free-boson system in more detail. This will enable us to choose a minimum value of m such that we get accurate numerical results. We also investigate the alternative approach where one starts from the continuum boson action and uses a trigonometric expansion of the coordinates to perform the integral over the imaginary-time variable.[6] We compare the rate of convergence of the corresponding energies and specific heats and show that the first formulation is superior for the numerical calculation of the path integral.

In the discrete formulation the partition function of the free-boson system is given by

$$Z_m^B=\left[\prod_{k=0}^{m-1} a_k^{-1/2}\right]^N , \tag{A1}$$

where a_k is given by (2.5c). The energy and specific heat per site are written as

$$E_m^B=\frac{\tau\Omega^2}{2m}\sum_{k=0}^{m-1} a_k^{-1} , \tag{A2}$$

and

$$C_m^B=\frac{(\tau\Omega)^4}{2}\sum_{k=0}^{m-1} a_k^{-2}-\frac{(\tau\Omega)^2}{2}\sum_{k=0}^{m-1} a_k^{-1} . \tag{A3}$$

In the continuum limit we start from the action

$$S=\tfrac{1}{2}\int_0^\beta dt[\dot{x}^2(t)+\Omega^2 x^2(t)] , \tag{A4a}$$

use the ansatz[6]

$$x(t)=b_0+\sum_{k=1}^{K-1} b_k \sin\frac{\pi k t}{\beta} , \tag{A4b}$$

and integrate over t. The functional integral over all paths $x(t)$ is now replaced by an integral over all possible values of b_k. Because the action S is quadratic in b_k it is straightforward to obtain[16]

$$Z_m=\int e^{-S}\mathscr{D}x=[\det(d_{ij})]^{-N/2} =\left[(1-D)\prod_{k=0}^{K-1} d_{kk}\right]^{-N/2} , \tag{A5a}$$

where

$$D=\sum_{k=1}^{K-1}\frac{d_{0k}^2}{d_{00}d_{kk}} , \tag{A5b}$$

$$d_{kk}=(\pi k)^2+(\beta\Omega)^2(1+\delta_{k,0}) , \tag{A5c}$$

$$d_{0k}=d_{k0}=2(\beta\Omega)^2\left[\frac{1-\cos k\pi}{k\pi}\right] , \tag{A5d}$$

and all other elements are zero. The energy and specific heat per site read

$$e_m=\frac{1}{\beta}\left[(\beta\Omega)^2\sum_{k=0}^{K-1} d_{kk}^{-1}(1+\delta_{k,0})-\hat{D}_2(1-D)^{-1}\right] , \tag{A6}$$

$$c_m=2(\beta\Omega)^4\sum_{k=0}^{K-1} d_{kk}^{-2}(1+\delta_{k,0})^2-(\beta\Omega)^2\sum_{k=0}^{K-1} d_{kk}^{-1}(1+\delta_{k,0})+2(\hat{D}_2)^2(1-D)^{-2}+(1-D)^{-1}[\hat{D}_2-4(\beta\Omega)^2\hat{D}_3] \tag{A7}$$

with

$$\hat{D}_n=\sum_{k=1}^{K-1}\frac{(k\pi d_{0k})^2}{d_{00}(d_{kk})^n} . \tag{A8}$$

Because a free-boson model can be solved exactly, we are in the unusual situation where we can take the limit $K\to\infty$ analytically. In the case of a more complex system this is not possible and we may regard the expansion (A4b) as an approximation. Then it is reasonable to set $K=m$ such that the

number of variables in the functional integrals is the same. Now we can compare these different approximations to the path integral of the free-boson model by calculating the energies (A2) and (A6) and specific heats (A3) and (A7) as a function of $K=m$ and β ($\Omega=1$ in our numerical calculations). The results for $\beta=5$ are given in Table I. The exact results corresponds to $m=\infty$. Comparing the exact energy with the exact ground-state energy equal to $\frac{1}{2}$ we may conclude that $\beta=5$ corresponds to a very low temperature. It is clear that the continuum formulation is inferior to the discrete formulation with regard to the rate of convergence. Because of the nature of the approximations we might expect that convergence is faster if the temperature is higher. This is illustrated in Table II where we give the results for $\beta=1$. Note also that, in this case, both approximations to the path integral yield lower bounds to the energy.

We conclude that although the trigonometric ansatz is very well suited to approximate the integral over the imaginary time t, it is not as good as the simple trapezium rule if the additional functional integral over all possible paths has to be performed.

APPENDIX B

Here we consider the case where the fermion-boson coupling is weak and calculate the energy by means of perturbation theory. We present the formalism in a notation appropriate for the 1D case, the extension to higher dimensionality is trivial. The Hamiltonian of the noninteracting system is

$$H_0=-\sum_k \epsilon_k c_k^\dagger c_k+\Omega\sum_k a_k^\dagger a_k\ , \tag{B1}$$

where $\epsilon_k=2t\cos k$. The interaction is given by

$$H_1=\frac{\lambda}{\sqrt{2\Omega}}\sum_k (a_{-k}^\dagger+a_k)\rho_k\ , \tag{B2}$$

where ρ_k denotes the Fourier-transformed fermion density. To second order in λ the Taylor expansion of the partition function reads

$$Z(\lambda)=Z_0+\frac{\beta}{2}Z_2\ , \tag{B3a}$$

$$Z_0=\mathrm{Tr}e^{-\beta H_0}\ , \tag{B3b}$$

$$Z_2=\int_0^\beta dx\ \mathrm{Tr}e^{(x-\beta)H_0}H_1 e^{-xH_0}H_1\ . \tag{B3c}$$

The first-order term is zero because H_1 changes the total number of bosons. We now evaluate Z_2/Z_0 by standard techniques and obtain

$$Z_2/Z_0=\frac{\lambda^2\Omega^{-1}}{e^{\beta\Omega}-1}\frac{1}{Z_0^F}\sum_{k,p}e^{\beta\epsilon_p}\frac{e^{\beta(\epsilon_k-\epsilon_p+\Omega)}-1}{\epsilon_k-\epsilon_p+\Omega}\ , \tag{B4a}$$

where

$$Z_0^F=\sum_p e^{\beta\epsilon_p} \tag{B4b}$$

is the partition function of the free fermion. The thermal energy is given by $E(\lambda)=E_0^B+E_0^F+E_2$ where E_0^B is the free-boson energy, E_0^F is the free-fermion energy, and

$$E_2=-\frac{1}{2}\frac{\partial}{\partial\beta}\beta\frac{Z_2}{Z_0} \tag{B5}$$

is the interaction energy. Using (B4a) we find

$$E_2=-\frac{1}{2}\frac{\lambda^2\Omega^{-1}}{e^{\beta\Omega}-1}\left[e^{\beta\Omega}+\left[1+E_0^F-\frac{\beta\Omega}{1-e^{-\beta\Omega}}\right]\frac{1}{Z_0^F}\sum_{k,p}e^{\beta\epsilon_p}\frac{e^{\beta(\epsilon_k-\epsilon_p+\Omega)}-1}{\epsilon_k-\epsilon_p+\Omega}+\frac{\beta}{Z_0^F}\sum_{k,p}\epsilon_p e^{\beta\epsilon_p}\frac{e^{\beta(\epsilon_k-\epsilon_p+\Omega)}-1}{\epsilon_k-\epsilon_p+\Omega}\right]\ . \tag{B6}$$

In general, the summations over k and p have to be done numerically. In the ground state ($\beta\to\infty$) (B6) reduces to

$$E_2=-\frac{\lambda^2}{2\Omega}\sum_p(\epsilon_0-\epsilon_p+\Omega)^{-1}\ , \tag{B7}$$

a result which could have been written down directly by using the lattice Green's functions.[15]

[1]H. De Raedt and A. Lagendijk, Phys. Rev. Lett. 49, 1522 (1982).

[2]T. Holstein, Adv. Phys. 8, 325 (1959); 8, 343 (1959); D. Emin, *ibid.* 22, 57 (1973).

[3]J. Appel, in *Solid State Physics,* edited by H. Ehrenreich, F. Seitz, and D. Turnbull (Academic, New York, 1968), Vol. 21.

[4]G. D. Mahan, *Many Particle Physics* (Plenum, New

York, 1981).
[5]J. M. Luttinger and Chih-Yuan Lu, Phys. Rev. B 21, 4251 (1980).
[6]R. P. Feynman and A. R. Hibbs, *Quantum Mechanics and Path Integrals* (McGraw-Hill, New York, 1965).
[7]N. Metropolis, A. W. Rosenbluth, M. N. Rosenbluth, A. H. Teller, and E. Teller, J. Chem. Phys. 21, 1087 (1953).
[8]J. M. Hammersley and D. C. Handscomb, *Monte Carlo Methods* (Methuen, London, 1964).
[9]K. Binder, in *Phase Transitions and Critical Phenomena,* edited by C. Domb and M. S. Green (Academic, New York, 1976), Vol. 5b.
[10]H. F. Trotter, Proc. Am. Math. Soc. 10, 545 (1959); M. Suzuki, Commun. Math. Phys. 51, 183 (1976).
[11]F. W. Wiegel, Phys. Rep. C 16, 2 (1975).
[12]S. Golden, Phys. Rev. 137, 1127 (1965); E. Lieb and W. Thirring, *Studies in Mathematical Physics* (Princeton University Press, Princeton, N.J., 1976).
[13]H. De Raedt and A. Lagendijk, Phys. Rev. Lett. 46, 77 (1981); J. Stat. Phys. 27, 731 (1982).
[14]J. E. Hirsch, D. J. Scalapino, R. L. Sugar, and R. Blankenbecler, Phys. Rev. Lett. 47, 1628 (1981); J. E. Hirsch, R. L. Sugar, D. J. Scalapino, and R. Blankenbecler, Phys. Rev. B 26, 5033 (1982).
[15]E. N. Economou, *Green's Functions in Quantum Physics* (Springer, Berlin, 1979).
[16]L. D. Fosdick, J. Math. Phys. 3, 1251 (1962).